arXiv:1610.03755v1 [cond-mat.mes-hall] 12 Oct 2016

Signatures of Chaos in Thermal Switching of Nanomagnets

M. d'Aquino[1], C. Serpico[2], S. Perna[2], A. Quercia[2], G. Bertotti[3], D.P. Ansalone[3], I.D. Mayergoyz[4]
[1]*Engineering Department, University of Naples "Parthenope", I-80143 Napoli, Italy.*
[2]*Dept. of EE and Information Technologies, University of Naples Federico II, I-80125 Napoli, Italy*
[3]*Istituto Nazionale di Ricerca Metrologica (INRIM), I-10135 Torino, Italy.*
[4]*ECE Department, University of Maryland, College Park, MD 20742, USA.*

Thermally-activated magnetization dynamics of small nanoparticles subject to microwave (AC) external fields is studied. It is shown that, under sufficiently strong microwave excitations, chaotic magnetization dynamics may occur close to saddle-type heteroclinic connections, and this heteroclinic chaos is responsible for the erosion of the safe basin around stable magnetization states. The erosion phenomenon is then connected to the escape problem from the energy well surrounding a stable equilibrium. It is shown that escape times follow a generalized Arrhenius' law governed by temperature, microwave field amplitude, frequency and heteroclinic chaos threshold.

The understanding of magnetization dynamics in nano-scale magnets subject to time-harmonic (AC) excitations is of crucial importance both from fundamental and application points of view [1, 2]. Anisotropic single-domain nanomagnets are important physical realizations of bistable systems affected by thermal fluctuations. These systems have been used as archetypal models in such research areas as stochastic resonance and AC-driven noise-induced escape[3, 4]. The theoretical understanding of physical phenomena in such systems is far from being complete especially when the frequency of AC excitation is large with respect to the thermal switching frequency[5, 6]. On the other hand, single-domain nanomagnets subject to AC excitations play a crucial role in magnetic storage technologies[7] especially in connection with the recently proposed technique of microwave assisted switching[8–10]. There are also other applications related to spin-valve nanomagnets excited by AC spin-polarized currents which are, for instance, very relevant in the design of novel MRAM cells with low operating power[11, 12].

Magnetization dynamics of uniformly magnetized particles subject to AC fields has been traditionally studied in connection with ferromagnetic resonance[13], where AC-driven magnetization oscillations are excited around a stable equilibrium corresponding to a system energy minimum. The small oscillation amplitude as function of frequency follows the usual resonance curve peaked around the Kittel frequency[13]. At somewhat larger AC powers, nonlinearity may lead to the fold-over phenomena which may result in frequency response hysteresis[14]. At larger AC excitation powers, the nonlinear response depends on the spatial dimensions of magnetic particles. In particles with linear dimensions from ten to hundred microns, spatially nonuniform spin-wave modes may couple with spatially uniform precessional magnetization dynamics giving rise to spin-wave instability phenomena[15]. This may lead to the appearance of spatially nonuniform regimes of quasi-periodic, chaotic, and turbulent-like nature[16, 17]. However, at the submicron scale, the spin-wave instability phenomena are strongly inhibited by exchange interactions[18]. For this reason, even at considerably large AC powers, nonlinear dynamics in nanomagnets exhibits mostly a spatially uniform mode of oscillations[19–21].

In this letter, we study AC-driven magnetization dynamics for single-domain bistable nanomagnets in the presence of weak thermal noise. In the previous studies of AC-driven magnetization dynamics, the existence of saddle points connected by separatrices has been completely ignored. However, the presence of saddle points leads to the enormous complexity in AC-excited magnetization dynamics where the chaotic behavior is often dominant. Below we study these physical phenomena with a special emphasis on the interplay between chaotic dynamics and thermal excitations. It is worthwhile to point out that linear response theory[22, 23] is not applicable to the study of this dynamics since the system is far from thermal equilibrium within the time scale of interest.

The main result of this paper is to demonstrate that chaotic saddle dynamics has measurable effects on thermal magnetization switching of nanomagnets. In particular, chaotic dynamics leads to the modification of the classical Brown-Arrhenius' law for escape times[24]. Namely, it is demonstrated that the prefactor appears in Arrhenius' law which depends on microwave field frequency and magnetic field amplitude threshold for the onset of chaotic saddle dynamics. Moreover, we show that, when escape times are plotted against the ratio of the AC-field amplitude to the AC-field threshold value for the onset of chaotic saddle dynamics, all the plots collapse onto one curve, which reveals some universality in the influence of escape times by chaotic saddle dynamics. We believe that the aforementioned effects are instrumental for the complete understanding of microwave assisted magnetization switching[25–27].

Magnetization dynamics for uniformly magnetized particles is described by the following stochastic Landau-Lifshitz equation[2, 22]

$$\frac{d\boldsymbol{m}}{dt} = -\boldsymbol{m}\times\boldsymbol{h}_{\rm eff} - \alpha\boldsymbol{m}\times(\boldsymbol{m}\times\boldsymbol{h}_{\rm eff}) - \mathbf{m}\times\nu\boldsymbol{h}_{\rm N}\,, \quad (1)$$

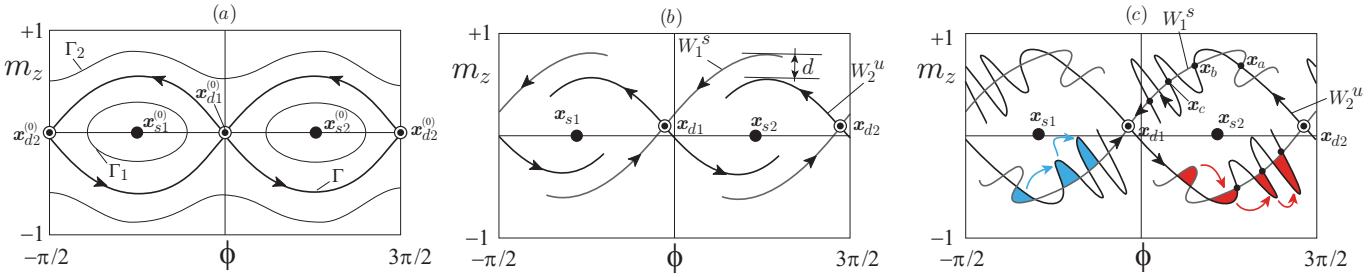

FIG. 1: Qualitative sketches of the separatrices associated to the stroboscopic map (see eq.(3)) in the (ϕ, m_z)-plane (where ϕ is the azimuth around the z-axis). (a) Unperturbed case (superscript notation $^{(0)}$ means $\alpha = 0, \boldsymbol{h}_a = 0$); (b) damping dominated dynamics; (c) Heteroclinic tangle formation. Legend: $\boldsymbol{x}_{d1}, \boldsymbol{x}_{d2}$ saddle equilibria; $\boldsymbol{x}_{s1}, \boldsymbol{x}_{s2}$ node-type equilibria; W_1^s stable manifold associated with $\boldsymbol{x}_{d1}$; W_2^u unstable manifold associated with $\boldsymbol{x}_{d2}$; d splitting of the manifolds; Γ heteroclinic trajectory in the conservative case, and Γ_1, Γ_2 are constant energy trajectories. The points $\boldsymbol{x}_a, \boldsymbol{x}_b, \boldsymbol{x}_c$ are generated by iterating the stroboscopic map. The colored arrows in (c) indicate the transformation of one lobe into another under the action of the maps: in blue capturing lobes, and in red escaping lobes are indicated respectively.

where $\boldsymbol{m}$ is the magnetization vector of unit length $|\boldsymbol{m}| = 1$ (normalized by the saturation magnetization M_s), time is measured in units of $(\gamma M_s)^{-1}$ (γ is the absolute value of the gyromagnetic ratio), $\boldsymbol{h}_{\text{eff}} = -\partial g/\partial \boldsymbol{m}$ is the effective field, $g = g(\boldsymbol{m}, \boldsymbol{h}_a(t))$ is the free energy, α is the damping constant, ν is the thermal noise intensity and $\boldsymbol{h}_{\text{N}}(t)$ is the standard isotropic Gaussian white-noise stochastic process. The energy function g, measured in units of $\mu_0 M_s^2 V$ (μ_0 is the vacuum permeability and V the volume of the particle), is given by:

$$g(\boldsymbol{m}, \boldsymbol{h}_a(t)) = g_0(\boldsymbol{m}) - \boldsymbol{h}_a(t) \cdot \boldsymbol{m}\,, \tag{2}$$

where $g_0(\boldsymbol{m}) = (D_x m_x^2 + D_y m_y^2 + D_z m_z^2)/2$, D_x, D_y, D_z are effective anisotropy constants and $\boldsymbol{h}_a(t)$ is time-harmonic (AC) external field. The intensity of the thermal noise ν is connected to the damping α in accordance with the fluctuation-dissipation theorem[2], i.e. $\nu^2 = (2\alpha k_B T)/(\mu_0 M_s^2 V)$, where T is the absolute temperature of the thermal bath and k_B is the Boltzmann constant.

Before discussing the interaction of chaotic saddle dynamics with thermal activation, we first describe the deterministic mechanism at the basis of chaotic saddle dynamics. To this end, we focus our attention on the case when thermal fluctuations are negligible, namely when $\nu = 0$ in eq.(1). Deterministic magnetization dynamics on the unit sphere described by eq.(1) (with $\nu = 0$) is a two dimensional dynamical system of nonautonomous type since the right-hand-side of the equation depends explicitly and periodically on time. This type of dynamics can be conveniently studied by introducing the stroboscopic map [28]:

$$\boldsymbol{m}_{n+1} = P[\boldsymbol{m}_n]\,, \tag{3}$$

where $\boldsymbol{m}_n = \boldsymbol{m}(t_0 + n\,T)$, and $T = 2\pi/\omega$, which maps an initial magnetization $\boldsymbol{m}(t_0)$ to the magnetization $\boldsymbol{m}(t_0 + T)$ obtained by integrating eq.(1) (with $\nu = 0$) over a time interval equal to the period T of the AC field. The mathematical form of the stroboscopic map cannot be derived in closed form, but certain features of the map dynamics can be obtained when the damping and the applied field are small. In this case, the map describes the perturbation of the conservative dynamics described by eq.(1) when $\alpha = 0$, $\boldsymbol{h}_a = 0$ and $\nu = 0$. The time evolution of magnetization in the conservative dynamics follows the constant level energy lines which are sketched in Fig.1(a). A crucial role in the map dynamics (3) is played by the saddles equilibria $(\boldsymbol{x}_{d1}^{(0)}, \boldsymbol{x}_{d2}^{(0)})$ heteroclinically connected by separatrices (Fig.1(a)). The saddle points of the map (see Fig.1(b)) are also at the origin of lines, referred to as stable and unstable manifolds, that give rise to the structuring of the state space. The stable manifolds W_1^s, W_2^s are sets (curves) of all initial conditions which under the action of the map (3) approach the saddles $\boldsymbol{x}_{d1}$, $\boldsymbol{x}_{d2}$, respectively. While the unstable manifolds W_1^u, W_2^u are sets (curves) of all initial conditions which under the backward in time action of the map (3) approach the saddles $\boldsymbol{x}_{d1}$, $\boldsymbol{x}_{d2}$, respectively. These manifolds are invariant sets, which means that they contain all forward and backward iterates of points taken on them.

In Fig.1(b), the two manifolds W_1^s and W_2^u are sketched and their splitting is indicated by d. This splitting depends on the value of damping and AC-fields and may vanish for sufficiently large AC perturbations. When this occurs, a point of intersection $\boldsymbol{x}_a$ belonging to both invariant sets W_1^s and W_2^u is realized (see Fig.1(c)). This implies that forward and backward iterates of $P[\cdot]$ starting from $\boldsymbol{x}_a$ must belong to $W_1^s \cap W_2^u$ and thus that the two curves W_1^s, W_2^u must intersect an infinite number of times (see Fig.1(c)). This phenomenon is referred to as chaotic saddle, and also as heteroclinic tangle, and is responsible for chaotic and unpredictable dynamic behavior of the system near the saddles. This chaotic dynamics can be explained in terms of lobe dynamics. Regions of the state space bounded by segments of stable and un-

stable manifolds of the saddles form lobes, examples of which are the colored regions in Fig.1(c). Under the action of the map, one lobe transforms into another. There are two classes of lobes: the escaping ones (indicated in red) which tend to bring point outside the well, and the capturing lobes (indicated in blue) which tend to bring points inside the well. Escaping and capturing lobes do actually finely intersect possibly a denumerable amount of times, and this gives rise to a fractal boundary between the points which enter the well and points which escape the well[28]. The intricacy of the intersection of lobes can be grasped by viewing Fig.2 in which stable and unstable manifolds of the map are numerically computed. The region in which lobes formed by the stable and unstable manifold intersect is the region where chaotic saddle dynamics takes place.

It turns out that, for sufficiently small applied fields and damping, the splitting d can be analytically derived by using the Melnikov function technique[29, 30] and one can estimate the threshold AC field[31, 32] at which the splitting becomes zero and the saddle becomes chaotic. In the special case of linearly polarized AC fields, namely when $\boldsymbol{h}_a(t) = \boldsymbol{e}_j h_{a,j}\cos(\omega t)$, with $\omega = 2\pi/T$, and with $\boldsymbol{e}_j$ denoting cartesian unit vectors, the threshold AC field as function of ω and geometrical/material parameters associated with the nanoparticle, is given by[33]:

$$h^{\rm crit}_{ac,j} = \frac{2\alpha\Omega_d}{|u_j(\omega)|}\,, \tag{4}$$

where $j = \{x, y, z\}$, $k^2 = (D_z - D_y)/(D_z - D_x)$, $k'^2 = 1 - k^2$, $\Omega_d = \sqrt{(D_z - D_y)(D_y - D_x)}$, $q = \omega/\Omega_d$ and

$$\boldsymbol{u}(\omega) = (s_x k \boldsymbol{e}_x + s_z k' \boldsymbol{e}_z)\frac{-{\rm i}\pi q}{\cosh\frac{\pi q}{2}} + s_x s_z \boldsymbol{e}_y \frac{\pi q}{\sinh\frac{\pi q}{2}}\,, \tag{5}$$

being $s_x, s_z = \pm 1$. A plot of $h^{\rm crit}_{ac,y}$ as a function of ω is reported in Fig.3(b). For field amplitudes significantly exceeding the threshold values (4), the region of chaotic dynamics expands and can penetrate deep into the basin of attraction surrounding the stable equilibria s_1, s_2 as it is evident in Fig.2.

The effect of the chaotic saddle and the presence of lobes lead to the deterministic escape of trajectory from the potential well around one of the free energy minima. This phenomenon is illustrated in Fig.3(a) by numerical simulations. These simulations are carried out for AC fields linearly polarized along the intermediate anisotropy axis y of the particle, but the same reasoning can be used for different field orientations. Thus, in the chosen situation, by using eq.(4), it is possible to compute analytically the threshold AC field amplitude $h^{\rm crit}_{ac,y}$ for the tangle, which ranges from 0.0055 to 0.017 for angular frequencies $\omega \in [0, 1]$ (see Fig.3(b)). We observe that, for the chosen parameters, the DC switching field related with the anisotropy energy barrier is

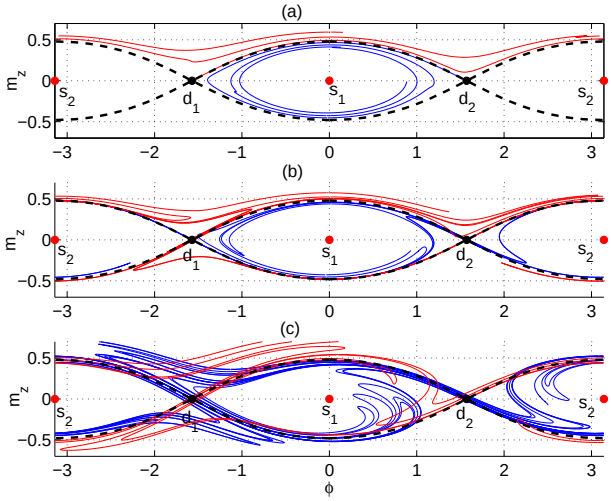

FIG. 2: Numerically computed W^u_2 and W^s_1 manifolds associated to the saddles of the stroboscopic map in the (ϕ, m_z) plane, for $n = 5$ iterates of the map. The AC field is linearly polarized along the y direction. Values of parameters: $D_x = -0.3, D_y = 0, D_z = 1, \alpha = 0.01, V = 3\times10^{-25}\,{\rm nm}^3$ (e.g. disk 1nm thick, with radius 10 nm and in-plane uniaxial anisotropy along x). Dashed lines refer to heteroclinic trajectories in conservative dynamics, the blue (red) line refers to W^u_2 (W^s_1). (a) $h_{ay} = 0.005$ smaller than the tangle threshold; (b) $h_{ay} = 0.01$ slightly larger than the tangle threshold; (c) $h_{ay} = 0.05$ much larger than the tangle threshold. The frequency coincides with the Kittel FMR frequency $\omega_K = \sqrt{(D_y - D_x)(D_z - D_x)} = 0.62$. The threshold computed from eq.(4) is $h^{\rm crit}_{ac,y}(\omega_2) = 0.0089$.

$D_{yx} = D_y - D_x = 0.3$, which is significantly higher than the AC field threshold in a very broad range of frequencies ($\mu_0 M_s = 1$T implies $\omega = 1 \to f \approx 28$GHz). More specifically, Fig.3(a) reports in (ϕ, m_z) plane, as function of ω and for constant AC field amplitude $h_{ay} = 0.05$, the initial magnetization states corresponding to particles which have not escaped the well within $n = 5$ iterates of the stroboscopic map. We have checked that choosing $n > 5$ does not significantly affect the results, which can be ascribed to the aforementioned fractal nature of the lobe dynamics[28].

One can see that very complex erosion patterns appear in the basin around the stable equilibrium ($\phi = 0, m_z = 0$). It is also clear that the effect of the erosion is non monotonic as function of frequency[34] and is much more pronounced for frequencies well below the Kittel frequency $\omega_K = 0.62$. Nevertheless, despite the appearance of such complicated basin erosion, for some frequencies, it is still possible to recognize in Fig.3(a) safe regions surrounding the stable equilibrium (e.g. for $\omega = 0.23, 0.30, 0.38, 0.62$). In general, one can be easily convinced that, in appropriate ranges of AC field amplitude and frequency, a safety region around the minimum of system free energy does exist. This region plays the role of a well in which attractive fixed points or attractive

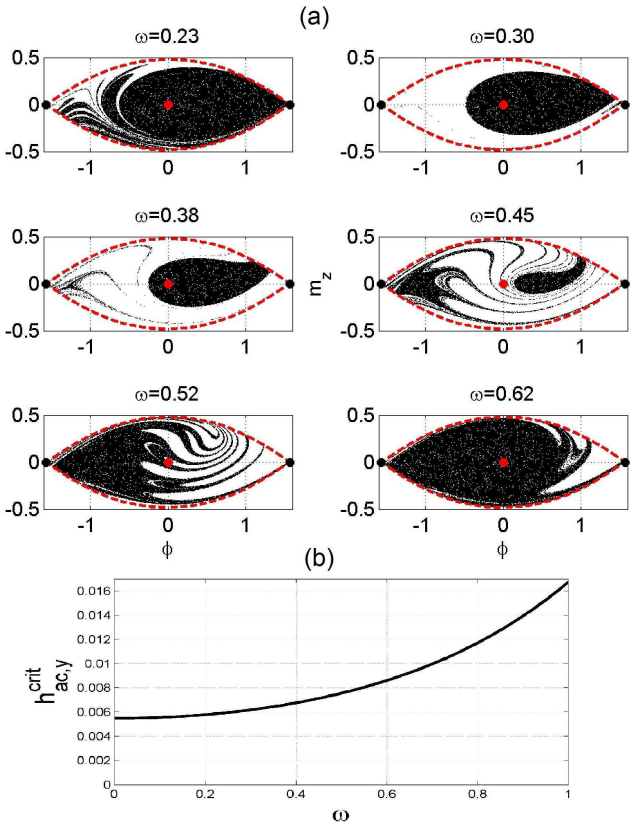

FIG. 3: (a) Basin erosion produced in the (ϕ, m_z)-plane for fields linearly polarized along y direction at given values of ω. The low energy well is initially filled by $N = 10^5$ phase points. When the trajectory originating from a phase point escapes the well within $n = 5$ iterations of the map (3), it is considered 'unsafe' and disregarded. The remaining phase points correspond to 'safe' initial conditions. Values of parameters are the same as Fig.2 and $h_{ay} = 0.05$. (b) AC field amplitude threshold for heteroclinic tangle versus ω (see eq.(4)).

periodic trajectories of the stroboscopic map lie. This well is the one from which one can define the concept of escape in AC-driven conditions.

The role of the chaotic saddle in the erosion of the safe basin around stable equilibria has been investigated[34] as a purely deterministic effect on the magnetization dynamics but, up to our knowledge, the interplay between such chaotic regime and thermal fluctuations has been completely overlooked in applied and theoretical magnetism. It is well-known that, in the absence of applied field, the thermal transition (escape) times are ruled by the Arrhenius' law:

$$\tau = \tau_0 \exp\left[\frac{\Delta E}{k_B T}\right] \quad , \tag{6}$$

where $\Delta E = \mu_0 D_{yx} M_s^2 V/2$ is the anisotropy energy barrier to overcome in order to have thermal switching of the particle, τ_0 is the prefactor and $1/\tau_0$ is the so-called attempt frequency[24]. In order to take into account the

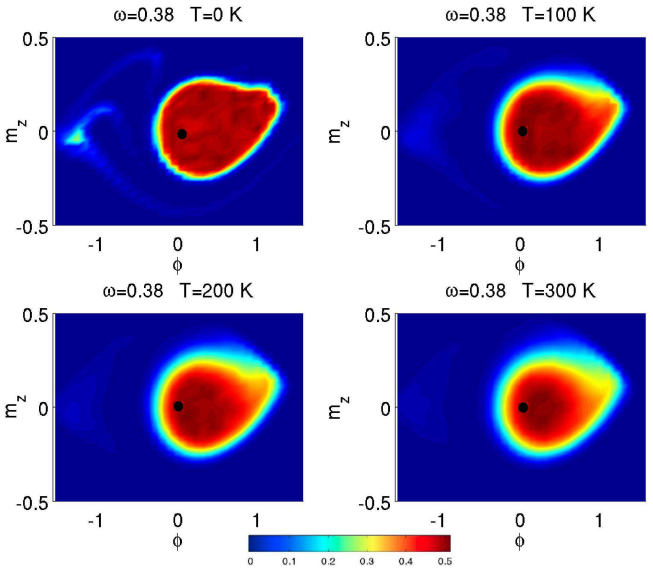

FIG. 4: (a) Basin erosion as function of temperature T. Color scale refers to particle density computed from the stroboscopic map at $n = 5$. Values of parameters same as Fig.2 and $h_{ay} = 0.05, \omega = 0.38$.

effect of AC excitations on escape times, we extend the concept of potential energy well in the presence of AC forcing by considering the safety regions associated with the erosion patterns (see Fig.3(a)).

The question that can be asked is whether and how the erosion pattern is affected by the thermal noise[35]. The answer to this question can be given by recomputing the stroboscopic map in the presence of thermal fluctuations in eq.(1). For sake of simplicity, we have performed such a computation for a given frequency $\omega \approx 0.38$ and increasing temperatures. The results are visible in Fig.4, where the basin erosion patterns, computed for $n = 5$ iterates and represented in terms of particle densities, are reported for temperatures $T = 0, 100, 200, 300$K. By comparing Figs. 3-4, one can see that, although the effect of temperature produces a smoothing of the tangling features, the safe basin around the stable state is still well-preserved, which is expected to yield nontrivial enhancement of thermal activation.

In order to relate the erosion of the energy well with the escape times, we have performed numerical simulations of thermally activated dynamics as function of the AC field amplitude, for frequencies $\omega_1 = 0.3$ and $\omega_2 = \omega_K = 0.62$ and $T = 250, 300$K. These frequency values have been intentionally chosen since the degree of erosion as function of h_{ay} is much larger for $\omega_1 = 0.3$ than that for $\omega_2 = 0.62$ (as it may be also inferred by comparing the tangle thresholds $h^{\rm crit}_{ac,y}(\omega_1) = 0.0062$ and $h^{\rm crit}_{ac,y}(\omega_2) = 0.0089$, respectively). For each particle replica starting from the initial state $m_x = 1$, the escape time has been determined by the condition $m_x < -0.9$. We have computed 100 realizations of the dynamics for

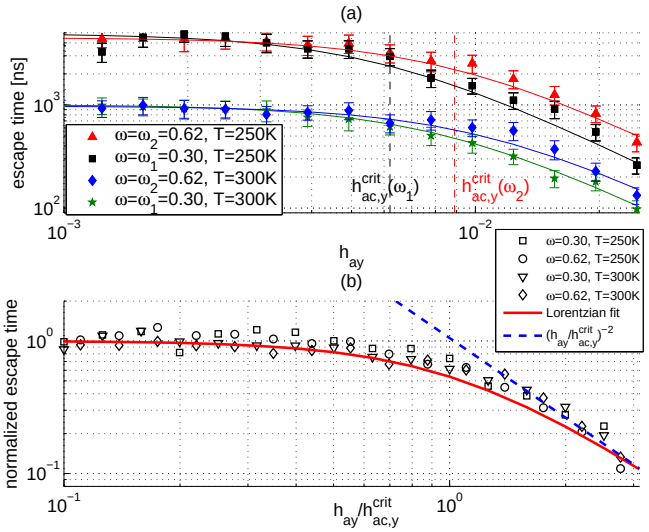

FIG. 5: (a) Escape time as function of AC field amplitude and frequency. Error bars refer to 95% confidence bounds; solid lines are fits with Lorentzian functions $p/(q+h_{ay}^2)$; (b) Scaling law for escape times vs normalized AC field $h_{ay}/h_{ac,y}^{\rm crit}(\omega)$; the solid line is a fit to a Lorentzian function $1/[1+\zeta(h_{ay}/h_{ac,y}^{\rm crit})^2]$, $\zeta = 0.86$. In both panels, symbols refer to different values of ω and T. Other parameters are the same as Fig.4.

each value of the AC field amplitude (100 points in the range $h_{ay} \in [0, 0.03]$) in order to get reliable statistics. The results are visible in Fig.5(a), where escape times are plotted in loglog scale against the AC field amplitude. One can see that, for each frequency and temperature, immediately above the tangle threshold, the escape times decrease following a scaling law with well-defined slope as function of the field amplitude. It is worth stressing that the tangle threshold is frequency-dependent.

In order to check whether the different obtained curves reflect a general behaviour, we have normalized the values of the escape time, for a given AC frequency and temperature, by the value (frequency-independent) of the escape time at the same temperature but with $h_{ay} = 0$. In addition, we have plotted the escape time as function of the ratio of h_{ay} and the threshold $h_{ac,y}^{\rm crit}(\omega)$. With these normalizations, all the different plots collapse onto one curve as shown in Fig.5(b). From this diagram, it is possible to infer that, for AC fields larger than the tangle thresholds, the thermal transition time scales as $\propto (h_{ay}/h_{ac,y}^{\rm crit})^{-2}$. This suggests that the escape time τ will follow a generalized Arrhenius' law

$$\tau(h_{ay},\omega) \approx \frac{\tau_0}{1+\zeta(h_{ay}/h_{ac,y}^{\rm crit}(\omega))^2} \cdot \exp\left[\frac{\Delta E}{k_B T}\right] \quad , \quad (7)$$

being ζ the only fitting parameter used.

Equation (7) reveals the physical meaning of the tangle threshold in thermally activated magnetization dynamics. In fact, it appears in the prefactor, which in the classical analysis of escape problem depends on the frequency of oscillations at the bottom of the energy well[24]. Conversely, here the microwave field excites far from equilibrium magnetization dynamics originating from the saddles. On one hand, we remark that, consistently with the classical Arrhenius' law, eq.(7) separates the effect of deterministic (microwave-driven) dynamics acting in the prefactor from the effect of thermal fluctuations controlling the height of the energy barrier. Nevertheless, on the other end, eq.(7) reveals their interplay, whose measurable signature is the prefactor scaling law expressed by the leading term in eq.(7) as function of the heteroclinic chaos threshold $h_{ac,y}^{\rm crit}$ at the frequency of the microwave field ω. In other words, we have shown that the heteroclinic chaos produces an effect similar to an artificial thermalization where the system is brought more often in condition to jump over the energy barrier.

The reduction of escape times by a quadratic term in h_{ay} is, for small h_{ay}, consistent with previous theoretical results[36]. However, the situation analyzed in Ref.[36] refers to resonant AC-driven dynamics at the bottom of the potential well, and the AC-induced corrections to escape times depend on the ratio between h_{ay} and an appropriately normalized temperature. Conversely, here far from equilibrium dynamics has been studied and the ratio $h_{ay}/h_{ac,y}^{\rm crit}(\omega)$ has been shown to control the reduction of escape times. A full theoretical justification of formula (7) goes beyond the limits of this paper. In fact, a combined theoretical and experimental study is currently in progress and will be the focus of future publications.

[1] J. Stoehr, H.C. Siegmann, Magnetism: From Fundamentals to Nanoscale Dynamics, Springer (2006).
[2] G. Bertotti, I. D. Mayergoyz, and C. Serpico, Nonlinear Magnetization Dynamics in Nanosystems, Elsevier, 2009.
[3] L.Gammaitoni, P. Haenggi, P. Jung, F. Marchesoni, Rev. Mod. Phys. **70**, 223 (1998)
[4] S.M. Soskin, R. Mannella and P.V.E. McClintock, Phys. Reports, **373** 247 (2003).
[5] V. N. Smelyanskiy, M. I. Dykman, H. Rabitz, and B. E. Vugmeister Phys. Rev. Lett. **79**, 3113 (1997).
[6] S. M. Soskin, R. Mannella, M. Arrayás, and A. N. Silchenko Phys. Rev. E **63**, 051111 (2001).
[7] S. Khizroev, D. Litvinov, Perpendicular Magnetic Recording, Springer (2005).
[8] J.-G. Zhu et al., IEEE Trans. Magn. 44, 125 (2008).
[9] S. Okamoto et al., J. Phys. D: Appl. Phys. 48, 353001 (2015).
[10] H. Suto et al., Phys. Rev. B 91, 094401 (2015).
[11] N. Locatelli et al., Nat.Mater. 13, 11 (2014).
[12] K.L. Wang, Proc. IEEE 104, 1974 (2016).
[13] C. Kittel, Phys. Rev. **73**, 155 (1948).
[14] D. J. Seagle et al., J. Appl. Phys. **57**, 15 (1965).
[15] H. Suhl, J. Phys. Chem. Solids 1, 209227 (1957).
[16] P. E. Wigen(Ed.), Nonlinear Phenomena and Chaos In Magnetic Materials, World Scientific Publishing, Singapore 1994.
[17] L'vov, Wave Turbulence Under Parametric Excitation, Springer (1994).

[18] G.Bertotti, I.D. Mayergoyz, and C.Serpico, Phys. Rev. Lett. **87**, 217203 (2001).
[19] L.F. Álvarez, O. Pla, O. Chubykalo, Phys. Rev. B **61**, 11613 (2000).
[20] Z. Li, Y.C. Li, S. Zhang, Phys. Rev. B **74**, 054417 (2006).
[21] G. Bertotti et al., J. Appl. Phys. **105**, 07B712 (2009).
[22] R. Kubo et al., Progr. Theor. Phys. Suppl., 46, 210 (1970).
[23] J.L. García-Palacios, F.J. Lázaro Phys. Rev. B **55**, 1006 (1997).
[24] W. F. Brown, Phys. Rev. 130, 1677 (1963).
[25] C. Thirion et al., Nature Mat. **2**, 524 (2003).
[26] M. d'Aquino et al., IEEE Trans. Magn. **45**, 3950 (2009).
[27] M. d'Aquino et al., J. Appl. Phys. **109**, 07D349 (2011).
[28] E. Ott, Chaos in Dynamical Systems. Cambridge University Press, 1997.
[29] P. Holmes, Phil. Trans. R. Soc. Lond. A **292**, 419-448 (1979).
[30] V.K. Mel'nikov, Trans. Moscow Math. Soc. **12**, 1 (1963).
[31] H. E. Nusse, J. A. Yorke, Physica D **36**, 137 (1989).
[32] E. Tyrkiel, Int. J. Bif. and Chaos **15**, 1215 (2005).
[33] C. Serpico, A. Quercia, G. Bertotti, M. d'Aquino, I. Mayergoyz, S. Perna, P. Ansalone, J. Appl. Phys. **117**, 17B719 (2015).
[34] M. d'Aquino et al., Physica B 486, 121-125 (2016).
[35] M.S. Soliman et al., Dynam. Stabil. Syst. 5, 281 (1990).
[36] S. Linkwitz, H. Grabert, Phys. Rev. B **44**, 11901 (1991)